

Review

Recent anode advances in solid oxide fuel cells

Chunwen Sun^{a,*}, Ulrich Stimming^{a,b}

^a Department of Physics E19, Technische Universität München, James-Frank Strasse 1, D-85748 Garching, Germany

^b Bavarian Center for Applied Energy Research (ZAE Bayern), Division 1, Walther-Meißner Strasse 6, D-85748 Garching, Germany

Received 9 January 2007; received in revised form 13 June 2007; accepted 17 June 2007

Available online 26 June 2007

Abstract

Solid oxide fuel cells (SOFCs) are electrochemical reactors that can directly convert the chemical energy of a fuel gas into electrical energy with high efficiency and in an environment-friendly way. The recent trends in the research of solid oxide fuel cells concern the use of available hydrocarbon fuels, such as natural gas. The most commonly used anode material Ni/YSZ cermet exhibits some disadvantages when hydrocarbons were used as fuels. Thus it is necessary to develop alternative anode materials which display mixed conductivity under fuel conditions. This article reviews the recent developments of anode in SOFCs with principal emphasis on the material aspects. In addition, the mechanism and kinetics of fuel oxidation reactions are also addressed. Various processes used for the cost-effective fabrication of anode have also been summarized. Finally, this review will be concluded with personal perspectives on the future research directions of this area.

© 2007 Elsevier B.V. All rights reserved.

Keywords: Solid oxide fuel cells; Anode materials; Microstructure; Reaction mechanism; Kinetics

Contents

1. Introduction	247
1.1. Basic operating principles of a SOFC	248
1.2. The anode three-phase boundary	249
2. The development of anode materials	249
2.1. Ni–YSZ cermet anode materials	249
2.2. Alternative anode materials	250
2.2.1. Fluorite anode materials	250
2.2.2. Perovskite anode materials	252
2.2.3. Tungsten bronze anode materials	254
2.2.4. Pyrochlore anode materials	254
2.3. Sulfur tolerant anode materials	255
3. The development of kinetics, reaction mechanism and models of anode	255
4. The development of cost-effective processing technologies for anode	257
5. Summary and outlook	258
Acknowledgments	258
References	259

1. Introduction

Fuel cells are devices for electrochemically converting the chemical energy of a fuel gas into electrical energy and heat without the need for direct combustion as an intermediate step, giving much higher conversion efficiencies than traditional energy con-

* Corresponding author. Tel.: +49 89 289 12527; fax: +49 89 289 12536.
E-mail address: csun@ph.tum.de (C. Sun).

version systems. In addition, this technology does not produce significant amounts of pollutants such as nitrogen oxides compared with internal combustion engines. Consequently, fuel cells are seen as more ideal energy sources in transport, stationary, and distributed power generators. The requirement of pure hydrogen or hydrogen-rich fuel is a major obstacle for commercial application of fuel cells.

The solid oxide fuel cells (SOFCs), based on an oxide-ion conducting electrolyte, have several advantages over other types of fuel cells, including relatively inexpensive materials, relatively low sensitivity to impurities in the fuel, and very high efficiency. Direct use available hydrocarbon fuels without first reforming them to hydrogen will greatly decrease the complexity and cost of the fuel cell system. Although the excellent electrocatalytic properties of the common used Ni/YSZ cermet materials in SOFCs for operation in H₂ fuel, they will suffer from carbon deposition and sulfur poisoning when hydrocarbon fuels are used [1–6]. Therefore, it is still facing great challenge for the development of new anode materials in SOFCs.

In recent years, there are intensive studies on the anode of solid oxide fuel cells, which are involved in many disciplinary fronts, mainly including materials, catalysis, surface science, and electrochemistry. This review aims to provide an overview of present research in the field of anode of SOFCs from materials to reaction mechanisms, to cost-effective fabrication processes. It will begin with a review of SOFCs operating principles. The emphasis will be placed on the development of anode material researches, especially for those that can directly utilize hydrocarbon fuels and tolerate sulfur.

1.1. Basic operating principles of a SOFC

Fig. 1 is a schematic diagram showing how SOFCs work. Starting from the cathode, molecular O₂ is first reduced to oxygen anions, using electrons external from the cell, in a half-cell reaction that can be written as follows:

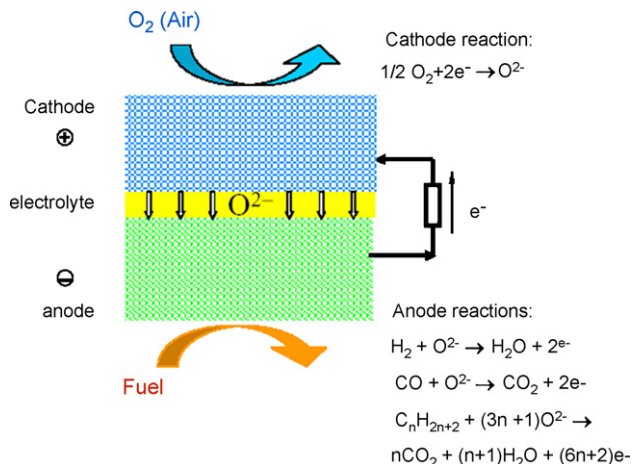
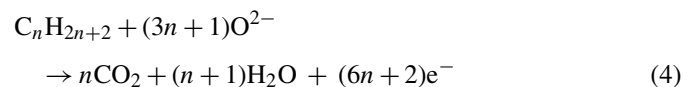


Fig. 1. Schematic diagram showing the working principle of a solid oxide fuel cell.

In order to accomplish this reaction, the cathode must be able to dissociate O₂ and be electronically conductive. The common cathode material is Sr-doped LaMnO₃ (LSM). In addition, there are lots of mixed ionic–electronic conductors (MIEC), which can be used as cathodes, such as, La_{0.6}Sr_{0.4}Fe_{0.8}Co_{0.2}O₃ [7,8], Ba_{0.5}Sr_{0.5}Co_{0.8}Fe_{0.2}O_{3–δ} [9], Sm_{0.5}Sr_{0.5}CoO₃ [10]. The ideal cathode materials should readily dissociate molecular oxygen, have high electronic and ionic conductivities, and have a coefficient of thermal expansion that matches with that of the electrolyte.

The electrolyte must be dense in order to separate the air and fuel compartments, must possess high ionic conductivity in order to allow easy migration of oxygen anions, and must be an electronic insulator. Furthermore, the electrolyte must maintain these properties over a wide range of $p(\text{O}_2)$, since the partial pressure of O₂ changes from ~ 1 atm at the cathode to $\sim 10^{-20}$ atm or lower at the anode [3]. The operating temperature for SOFCs is largely determined by the temperature required to achieve sufficient ionic conductivity in the electrolyte. The most commonly used electrolyte material is yttria-stabilized zirconia (YSZ). Some other oxides, such as doped ceria, La_{0.9}Sr_{0.1}Ga_{0.8}Mg_{0.2}O_{2.85} (LSGM), are also under consideration because they have higher ionic conductivities [1]. To date, however, YSZ continues to be the material of choice because it is stable over a wide range of $p(\text{O}_2)$, has reasonable mechanical strength, and is inexpensive. Because decreased operating temperatures simplify the material requirements in other parts of the SOFC, there is a trend toward using electrode supported thin electrolyte structures.

The anode not only functions as the sites for the electrochemical oxidation of the fuel, but also transfers charge to a conducting contact. Driven by the difference in oxygen chemical potential between fuel and air compartments of the cell, oxygen anions migrate through the electrolyte to the anode where they are consumed by oxidation of the fuel according to the following reactions:



Therefore, the catalytic properties of the anode to the fuel oxidation reaction are important. In addition, the anode materials must be compatible (chemical and thermal expansion) with other components (the electrolyte and interconnect). The anode must also provide paths for transport of gas from the fuel, electrons to the interconnect, and provide for the reactions of the oxygen ions from the electrolyte. In conventional designs using YSZ as the electrolyte, H₂ or the mixture of CO and H₂ as a fuel, the anode is a ceramic-metallic composite of nickel and YSZ (usually referred to as a “cermet”). In additions, other mixed ionic and electronic conducting oxides have also been used as the anode, which will be discussed later.

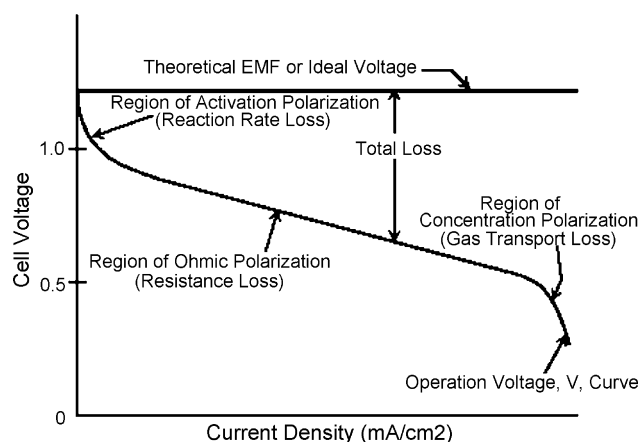


Fig. 2. Ideal and actual fuel cell voltage–current characteristic [12].

The ideal voltage (E^0) from a single cell under open circuit conditions (OCV) is calculated to be 1.01 V at 800 °C from the Nernst equation with pure hydrogen at the anode and air at the cathode [11]. However, the actual voltage output (V) under load conditions is usually lower than E^0 , given by

$$V = E^0 - IR - \eta_c - \eta_a \quad (5)$$

where I is the current through the cell, R the cell resistance, and η_c and η_a are the polarization losses associated with the cathode and anode, respectively. The voltage decrease is caused by several types of irreversible losses, as shown in Fig. 2 [12]. Multiple phenomena contribute to the irreversible losses in an actual fuel cell. These losses can be minimized by optimizing the properties of various components in a fuel cell, such as microstructure, exchange kinetics, transport properties, and so on.

In high-temperature fuel cells, the activation-related losses are often much less significant, and hence the characteristic concave portion of the V – I curve is hard to distinguish. In addition, as transport-related losses play a more important role, the convex portion of the curve often extends further to the left.

1.2. The anode three-phase boundary

The performance of a SOFC depends strongly on the anode structure which is mainly determined by the fabrication method. In addition, electrochemical reactions are quite different from normal heterogeneous reactions in some aspects [13]. Therefore, it is necessary to consider how the anode works on a microscopic scale [14,15]. It is well known that the electrochemical reaction can only occur at the three-phase boundary (TPB), which is defined as the collection of sites where oxygen ion conductor (the electrolyte), the electron-conducting metal phase, and the gas phase all meet together. A schematic illustration of the region between the electrolyte and the anode where the TPB exists is shown in Fig. 3 [3]. If there is a breakdown in connectivity in any one of the three phases, the reaction cannot occur. If ions from the electrolyte cannot reach the reaction site, if gas-phase fuel molecules cannot reach the site, or if electrons cannot be removed from the site, then that site cannot contribute to the performance of the cell. While the structure

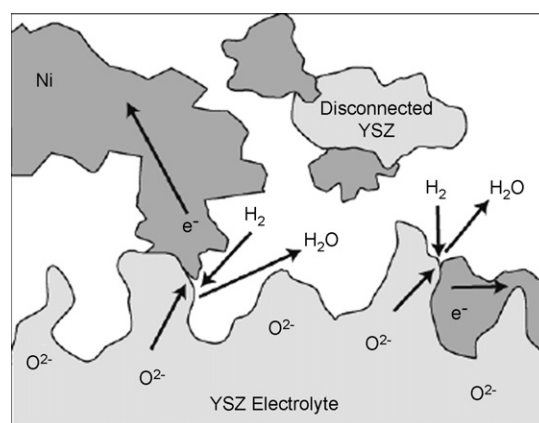


Fig. 3. Schematic diagram of Ni/YSZ anode three-phase boundary [3].

and composition clearly affect the size of the TPB, various theoretical and experimental methods have been used to estimate that it shortens no more than approximately 10 μm from the electrolyte into the electrode [3,13,16,17]. Essentially, so long as the diffusion of ions through the electrolyte partially limits the performance, the concentration of excess ions in the oxide phase of the anode will be insignificant. The TPB concept has important implications for the optimization of both anodes and cathodes. State-of-the-art fuel cell electrodes typically have a complex micro/nano-structure involving interconnected electronically and ionically conducting phase, gas phase porosity, and catalytically active surfaces [18,19].

2. The development of anode materials

2.1. Ni–YSZ cermet anode materials

The Ni in the cermet anode provides electronic conductivity and catalytic activity, both for direct oxidation and for steam reforming of methane. The YSZ provides a thermal expansion match with the YSZ electrolyte and also ionic conductivity to extend the reaction zone in the anode, in addition to function as a structural support for the anode that prevents Ni sintering [1–4]. Because NiO and YSZ do not form solid solutions, even at high temperatures, this green body can be sintered to form a NiO–YSZ composite and then reduced to form a porous Ni–YSZ cermet [20]. The amount of Ni is typically at least 30 vol.% to achieve the percolation threshold for electronic conductivity [21]. This material fulfils most requirements of the anode. The disadvantages of this material are its poor redox stability, low tolerance to sulphur [22], carbon deposition when using hydrocarbon fuels and the tendency of nickel agglomeration after prolonged operation. Especially, the low tolerance for carbon deposition makes this material inappropriate for operation with available hydrocarbon fuels [1–6,23]. Since nickel is an excellent catalyst for both steam reforming and hydrogen cracking, carbon deposition occurs rapidly when hydrocarbon was used as the fuel, unless excess steam is present to ensure steam reforming. The composition of the anode, particle sizes of the powders and the manufacturing method are crucial to achieving high electronic conductivity, adequate ionic conductivity, and

high activity for electrochemical reactions, reforming and shift reactions.

In general, to solve the problem of carbon deposit when using hydrocarbon fuels, several methods have been adopted. Firstly, the carbon deposition can be avoided by reducing operating temperature. Steele et al. [24] found that carbon arising from the dissociation of CH_4 is not deposited on many oxides until the temperature exceeds about 750°C . Murray et al. [25] deposited a $0.5\ \mu\text{m}$ thick $(\text{Y}_2\text{O}_3)_{0.15}(\text{CeO}_2)_{0.85}$ (YDC) porous film between YSZ electrolyte and Ni–YSZ anode using dc reactive magnetron sputtering. They achieved direct electrochemical oxidation of methane in solid oxide fuel cells at lower temperature. The power density is $0.37\ \text{W cm}^{-2}$ at 650°C and no carbon deposition was observed. However, Ni–ceria was used successfully only with methane and at relatively low temperatures.

Secondly, it can be avoided by improving the present anode materials. For example, a composite anode consisting of Cu– CeO_2 –YSZ/SDC demonstrated that the addition of CeO_2 to Cu–YSZ/SDC cermet significantly enhanced the performance of the cell, especially for hydrocarbon fuels [26–30]. It is suggested that CeO_2 promotes hydrocarbon oxidation. Typically, Gorte et al. [31] replaced Ni cermets with composites containing Cu and ceria or samaria-doped ceria. Unlike Ni, Cu is not catalytically active for carbon deposition but is effective as a current collector, while ceria provides a high catalytic activity for hydrocarbon reforming due to its oxygen storage and transport properties. They reported the direct, electrochemical oxidation of various hydrocarbons (methane, ethane, 1-butene, *n*-butane and toluene) at 973 and 1073 K. Gas phase pyrolysis reactions can still lead to tar formation on Cu cermet, however, the compounds that form on Cu tend to be polyaromatics rather than graphite. It has been suggested that these compounds enhance anode performance by providing additional electronic conductivity in the anode.

However, Cu is not good as an electrocatalyst as Ni, and power densities reported for thin YSZ electrolyte SOFCs with Cu-based anodes are lower than that for Ni-based anodes. In addition, Cu is a relatively low melting point metal, and is thus not compatible with many standard high-temperature SOFC fabrication techniques. One way of enhancing the activity and stability of Cu-based anodes involves alloying the Cu with a second metal that has higher catalytic activity, for which nickel seems to be a better choice [11]. Kim et al. [32] tested a range of Cu/Ni alloys at 800°C in CH_4 , with a composition of 0, 10, 20, 50 and 100% Ni. It was found that although small carbon deposits were formed there was an increase in power density over time. The increase in power density was attributed to an increase in electronic conductivity in the anode, and it implied the benefits of a small amount of carbon to fuel cell performance. They also observed that the Cu/Ni alloys display very different properties to either Ni-based or Cu-based cermets. Lee et al. [33] examined the performances of anodes containing mixtures of Cu and Ni or Cu and Co operated with both H_2 and *n*-butane fuels at 973 and 1073 K. The bimetallic anodes exhibited improved performance in H_2 at 973 K compared to Cu-based anodes and decreased carbon formation in *n*-butane compared to Ni- or Co-based anodes. In comparison, the Cu–Co appears to be more tolerant to car-

bon formation, possibly because Cu and Co are largely kept in separate phases. These results suggest that bimetallics are worth considering for fuel cells that operate on hydrocarbons. Xie et al. [34] further studied the performances of fuel cells consisting of a tri-metal alloy of $\text{Fe}_x\text{Co}_{0.5-x}\text{Ni}_{0.5}/\text{Sm}_{0.2}\text{Ce}_{0.8}\text{O}_{1.9}$ (SDC) cermet, CGO electrolyte and $\text{Sm}_{0.5}\text{Sr}_{0.5}\text{CoO}_3$ /SDC cathode. They found the fuel cells consisting of the tri-metal anode showed the lowest interfacial resistance and highest power density, and with $x = 0.25$ a much better electrochemical performance than that of Ni/SDC was observed.

Thirdly, it can be alleviated or avoided by looking for alternative anode materials, mainly including some fluorite, perovskite, tungsten bronze, and pyrochlore structure materials, which will be discussed in the following sections.

2.2. Alternative anode materials

In the context of direct utilization of available hydrocarbon fuels in SOFCs, the materials with mixed ionic and electronic conducting oxide may be desirable. The mixed conductivity extends the active zones that electrochemical reactions can occur by allowing O^{2-} ions to any position of interfaces between the anode and gas phase.

2.2.1. Fluorite anode materials

Other materials such as conductive oxides have been proposed as possible SOFC anode materials. Until now, most SOFC developers used doped ceria as the anode material to lower the operating temperature. Ceramics based on CeO_2 exhibit mixed ionic and electronic conductivity in a reducing atmosphere due to reduction of Ce^{4+} to Ce^{3+} . In addition, it is believed that the excellent catalytic activity of CeO_2 based materials stemmed from the oxygen-vacancy formation and migration associated with reversible CeO_2 – Ce_2O_3 transition [35,36]. It has been reported that ceria-based ion conductors [37] have a high resistance to carbon deposition, which permits the direct supply of dry hydrocarbon fuels to the anode. The more effective method, however, is the addition of Ni, Co and some noble metals, such as Pt, Rh, Pd and Ru, which are beneficial to the reforming reactions of hydrocarbon, due to their functions of breaking the C–H bond more easily, especially for the case of Ru [38,39].

Hibino et al. [40,41] studied a thin ceria-based electrolyte film SOFC with a Ru–Ni–GDC ($\text{Ce}_{0.9}\text{Gd}_{0.1}\text{O}_{1.95}$) anode that was directly operated on hydrocarbons, including methane, ethane, and propane, at 600°C . They claimed that the role of the Ru catalyst in the anode reaction was to promote the reforming reactions of the not reacted hydrocarbons by the produced steam and CO_2 , which avoided interference from steam and CO_2 in the gas phase diffusion of the fuels. The resulting peak power density reached $750\ \text{mW cm}^{-2}$ with dry methane, which was comparable to the peak power density of $769\ \text{mW cm}^{-2}$ with wet (2.9 vol.% H_2O) hydrogen.

Most recently, Barnett group reported a new SOFC that combines a Ru– CeO_2 catalyst layer with a conventional anode, allowing internal reforming of iso-octane without coking, making this solid oxide fuel cell a promising candidate for practical

and efficient fuel cell applications [42]. The fuel cell with SDC ($\text{Ce}_{0.85}\text{Sm}_{0.15}\text{O}_{1.925}$) as electrolyte yielded maximum power densities of $\sim 0.35 \text{ W cm}^{-2}$ at 570°C , a value comparable to those reported for other SDC based electrolyte cells operated on H_2 . However, as pointed by the authors, one of the drawbacks to the catalyst layer is that it reduces the rate at which fuel can diffuse to the anode, thereby decreases cell power density. Sun et al. [43] improved the structure of the fuel cells by using a flowerlike mesoporous CeO_2 microsphere as a catalyst support. It was found that the performance of the fuel cell used CeO_2 -Ru microsphere catalyst layer is obviously improved, producing maximum power density up to 0.654 W cm^{-2} at 600°C . Electrochemical impedance spectroscopy (EIS) analysis showed the kinetic characteristic of anode reactions in the fuel cell with porous CeO_2 -Ru microsphere catalyst layers was significantly enhanced.

Ramirez-Cabrera et al. [44] studied gadolinium-doped ceria, $\text{Ce}_{0.9}\text{Gd}_{0.1}\text{O}_{1.95}$ (CGO) as an anode material at 900°C in 5% CH_4 with steam/methane ratios between 0 and 5.5. The results revealed this material is resistant to carbon deposition; the reaction rate was controlled by slow methane adsorption. Marina et al. [37] studied the same catalyst for methane oxidation. It was also demonstrated that ceria has a low activity for methane oxidation but a high resistance to carbon deposition.

Antonucci et al. [45] investigated a Ru/CGO electrocatalyst combined with a Cu current collector for the direct electrooxidation and internal reforming of propane in a solid oxide fuel cell. Comparable electrochemical power densities for both direct oxidation and internal reforming have been measured at 750°C . They found that the electrochemical performance in the presence of propane was significantly affected by the polarization resistance which is about four times larger than that obtained for the SOFC fed with hydrogen. However, out-of-cell steam reforming tests showed a C_3H_8 conversion to syngas approaching 90% at 800°C . No carbon deposits was observed both upon operation of the anode in the direct oxidation and internal reforming process at 750°C .

Hibino et al. [46] studied the electrocatalytic oxidation of methane over anodes (0–10 wt.% Pd–30 wt.% $\text{Ce}_{0.8}\text{Sm}_{0.2}\text{O}_{1.9}$ -Ni) in a single-chamber SOFC, with a mixture of methane and air between 450 and 550°C . They found the addition of small amount of Pd to the anode significantly promoted the oxidation of methane by oxygen to form hydrogen and carbon monoxide, which resulted in electromotive forces of ca. 900 mV from the cell and extremely small electrode-reaction resistances of the anode. At 550°C , the peak power densities reached 644 mW cm^{-2} when a 0.15 mm thick SDC electrolyte was used.

Ahn et al. [47] examined the properties of Cu-ceria composite anode by replacing CeO_2 with a $\text{Ce}_{0.6}\text{Zr}_{0.4}\text{O}_2$ solid solution. They found that $\text{Ce}_{0.6}\text{Zr}_{0.4}\text{O}_2$ improved the thermal stability of anode, which is assigned to the improved reducibility of the solid solution compared to that of pure ceria.

Wisniewski et al. [48] tested $\text{Ir/Ce}_{0.9}\text{Gd}_{0.1}\text{O}_{2-x}$ for CO_2 reforming of CH_4 at 600 – 800°C , with CH_4 : CO_2 ratios between 2 and 0.66. They found that the catalyst showed good stability over 20 h, and no carbon formation was observed except in very

severe conditions of CH_4 : $\text{CO}_2 = 2$ at 800°C . However, they did not report comparison of the anode performance to that of Ni- or Cu-based cermets.

Recently, Ye et al. [49] investigated the performance of Cu-CeO₂-ScSZ (Scandia stabilized zirconia) composite anode for a SOFC running on ethanol fuel. They found the fuel cell with 21.5 wt.% Cu–8.5 wt.% CeO₂-ScSZ anode showed the best performance. At 800°C , this anode showed a stable performance for stream of ethanol and water, after 50 h operation on ethanol steam, the cell almost kept the same power output at 210 mW cm^{-2} and there was no visible carbon deposition on the anode surface after operation, but the mechanism of ethanol oxidation is still not understood.

For extending the regions that electrochemical reactions can occur, the introduction of transition metal oxides, e.g., TiO_2 , into a zirconia solid solution for use as anode materials is a promising strategy. Such materials display reasonable electrochemical activity that is comparable to that of ceria doped with 40% Gd. Tao et al. [50] found that TiO_2 may be dissolved to about 18 mol % in ternary systems Y_2O_3 - ZrO_2 - TiO_2 and Sc_2O_3 - ZrO_2 - TiO_2 , and 20 mol % in the quaternary system Sc_2O_3 - Y_2O_3 - ZrO_2 - TiO_2 . The ionic conductivity is related to the oxygen vacancy concentration and the size of dopant ions, and electronic conductivity to the lattice parameter, the sublattice ordering, as well as the degree of Ti substitution. Small lattice parameters are beneficial to electron hopping, resulting in higher electronic conductivity. They found that introduction of scandium into the Y_2O_3 - ZrO_2 - TiO_2 system has significantly improved both ionic and electronic conductivities. The highest ionic conductivity ($1.0 \times 10^{-2} \text{ S cm}^{-1}$ at 900°C) and electronic conductivity (0.14 S cm^{-1} at 900°C) were observed for $\text{Sc}_{0.2}\text{Zr}_{0.62}\text{Ti}_{0.18}\text{O}_{1.9}$ and $\text{Sc}_{0.1}\text{Y}_{0.1}\text{Zr}_{0.6}\text{Ti}_{0.2}\text{O}_{1.9}$, respectively. Considering the required levels of both ionic and electronic conductivities for ideal SOFC anode materials, $\text{Sc}_{0.15}\text{Y}_{0.05}\text{Zr}_{0.62}\text{Ti}_{0.18}\text{O}_{1.9}$ seems to be a promising candidate.

Kobayashi et al. [51] investigated the partial conductivities of electrons and holes in YSZ doped with 5 mol % of TiO_2 . The result is the partial conductivities of holes, σ_p , and electrons, σ_n , were proportional to $p_{\text{O}_2}^{1/4}$ and $p_{\text{O}_2}^{-1/4}$, respectively, except for σ_n in the low $p(\text{O}_2)$ regime. The partial conductivity of electrons, σ_n , was greater than that in non-doped one.

Wang et al. [52] investigated the performances of Tb and Ti doped YSZ mixed conducting electrode in thin-film YSZ cells. They found Tb and Ti doped YSZ enhance cell power densities from 15 to 50% at 800°C .

Hirabayashi et al. [53] studied doped Bi-based oxides as potential anode materials for direct hydrocarbon solid oxide fuel cells. It was found that $(\text{Bi}_2\text{O}_3)_{0.85}(\text{Ta}_2\text{O}_5)_{0.15}$ showed a promising candidate at intermediate temperatures (600°C). A fraction of Bi_2O_3 in this material was reduced to BiO and Bi metal under fuel conditions, which yielded higher mixed conductivity and sufficient catalytic activities to promote complete oxidation of hydrocarbons. No carbon deposition was observed when butane was used as the fuel below 800°C . In addition, this anode material was stable to both fuel and air and could avoid carbon deposition.

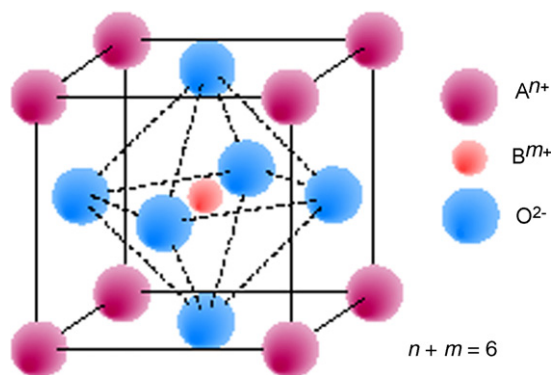


Fig. 4. Unit cell of the ABO_3 perovskite structure [54].

2.2.2. Perovskite anode materials

The perovskite-type oxide has the general formula ABO_3 , in which A and B are cations with a total charge of +6. The lower valence A cations (such as, La, Sr, Ca and Pb, etc.) are large and reside on the larger spaces in the 12-fold oxygen coordinated holes, the B cations (such as, Ti, Cr, Ni, Fe, Co and Zr, etc.) occupy the much smaller octahedral holes (six fold coordination). Full or partial substitution of the A or B cations with cations of different valence is possible. When the overall valence of the A-site and B-site cations ($n + m$) adds up to less than 6, the missing charge is made up by introducing vacancies at the oxygen lattice sites [54]. Fig. 4 shows the typical structure of the cubic perovskite ABO_3 . Recently, a lot of new compounds with perovskite structure have been offered as alternative anode materials in SOFCs.

Tao et al. [55] reported an oxygen-deficient perovskite $La_{0.75}Sr_{0.25}Cr_{0.5}Mn_{0.5}O_3$, with comparable electrochemical performance to that of Ni/YSZ cermet and with good catalytic activity for the electro-oxidation of CH_4 at high temperatures. The electrode polarization resistance approaches $0.2 \Omega \text{ cm}^2$ at 900°C in 97% $H_2/3\% H_2O$. Very good performance is achieved for methane oxidation without using excess steam. The anode is stable in both fuel and air conditions, and shows stable electrode performance in methane. Both redox stability and operation in low steam hydrocarbons have been demonstrated, overcoming two of the major limitations of the Ni-YSZ cermet anodes. However, $La_{0.75}Sr_{0.25}Cr_{0.5}Mn_{0.5}O_3$ has a low electronic conductivity in the reducing anodic atmosphere and is not stable to sulfur impurities in the fuel [56], even when impregnated with CuO to improve the electronic conductivity in the reducing atmosphere at the anode, the long-term performance has been proven unsatisfactory [57]. Nevertheless, their work pioneered the use of an oxygen-deficient, mixed-valence perovskite as a MIEC for the anode material of a SOFC. These oxides also have a thermal-expansion coefficient that is compatible with that of the solid oxide electrolyte.

Recently, Goodenough et al. [58] reported identification of the double perovskite $Sr_2Mg_{1-x}Mn_xMoO_{6-\delta}$ that can be used with natural gas as the fuel under operating temperatures $650^\circ\text{C} < T < 1000^\circ\text{C}$ with long-term stability and tolerance to sulfur. This material is characteristic of oxygen deficient and is stable in reducing atmosphere. The mixed valence

Mo(VI)/Mo(V) sub-array provides electronic conductivity with a large enough work function to accept electrons from a hydrocarbon. As a MIEC that can accept electrons while losing oxygen, it also promises to be catalytically active to the oxidation of H_2 and hydrocarbons. The ability to lose oxygen while accepting electrons is realized because Mo(VI) and Mo(V) form molybdenyl ions, which makes them stable in less than sixfold oxygen coordination, and both Mg^{2+} and Mn^{2+} are stable in fourfold as well as sixfold oxygen coordination [57]. The maximum power density reached 438 mW cm^{-2} for $Sr_2MgMoO_{6-\delta}$ at 800°C with dry CH_4 as the fuel.

Vernoux et al. [59] studied the catalytic and electrochemical characteristics of $La_{0.8}Sr_{0.2}Cr_{0.97}V_{0.03}O_3$ (LSCV). They found this material exhibited a low activity towards CH_4 steam reforming at 800°C , although it has been shown to be stable over time and does not suffer from carbon deposition. When Ru as a steam reforming catalyst was added to this electrode to implement the gradual internal reforming process, the LSCV-YSZ composite was a promising anode material.

Ruiz-Morales et al. [60] demonstrated symmetrical fuel cells (SFCs) using simultaneously the same material $La_{0.75}Sr_{0.25}Cr_{0.5}Mn_{0.5}O_{3-\delta}$ (LSCM) at the anode and cathode sides. Due to its enhanced electrochemical properties in both reducing and oxidizing conditions, LSCM-based SFCs offered promising performances, 0.5 and 0.3 W cm^{-2} at 950°C using H_2 and CH_4 as fuels, respectively.

Sauvet et al. [61] have studied the electrochemical properties of $La_{1-x}Sr_xCr_{1-y}Ru_yO_3$ ($x=0.2, 0.3, 0.4$ and $y=0.02, 0.05$) in hydrogen and methane fuel at 750 and 850°C . They found the best performances were obtained with 30% of strontium doping; variation of the ruthenium content, approximately between 0.02 and 0.05, had little influence on the electrochemical results. The electrochemical properties output were considerably improved by using a graded electrode and by surface coating the electrolyte with a thin ceria layer, approximately $5 \mu\text{m}$. For a ceria thickness higher than $5 \mu\text{m}$, the electrochemical performance was lower than that without the intermediate layer. At 750°C , the polarization resistance was $3.7 \Omega \text{ cm}^2$ in hydrogen and $40 \Omega \text{ cm}^2$ in methane for the YSZ/ CeO_2 /graded $La_{0.7}Sr_{0.3}Cr_{0.95}Ru_{0.5}O_3$ -YSZ structure. Sauvet et al. [62,63] also studied $La_{1-x}Sr_xCr_{1-y}Ni_yO_{3-\delta}$ compositions as a novel anode. They found these materials have some catalytic activity, although less than that of Ni composites. For methane steam reforming, no carbon deposition was observed when the ratio of steam to methane is 1 or less.

Liu et al. [64] investigated the performances of composite anodes consisting of an electronically conducting ceramic, $La_{0.8}Sr_{0.2}Cr_{0.8}Mn_{0.2}O_{3-\delta}$, an ionic conducting ceramic, $Ce_{0.9}Gd_{0.1}O_{1.95}$ (GDC), and a small fraction Ni in a SOFC with H_2 , CH_4 , C_3H_8 , and C_4H_{10} fuels, respectively. They found that the anode performance was comparable to that for Ni-GDC anodes with hydrogen and methane fuels. The anodes also provided good performance with propane and butane and, unlike Ni-GDC, there was little or no coking. The 4 wt.% Ni content in the anode was necessary to obtain good performance, indicating that a small amount of Ni provides a substantial electrocatalytic effect while not causing coking. Initial cell test results showed

good cell stability and indicated that the anodes were not affected by cyclic oxidation and reduction.

Jiang et al. [65] studied GDC-impregnated ($\text{La}_{0.75}\text{Sr}_{0.25}$) ($\text{Cr}_{0.5}\text{Mn}_{0.5}$) O_3 (LSCM) as an alternative Ni-free anode for the direct utilization of methane in solid oxide fuel cells. They found that impregnation of submicrometer and ionic conducting GDC greatly improves the electrocatalytic activity of the LSCM anodes for the oxidation reaction in weakly humidified (3% H_2O) methane. At 800 °C, electrode polarization resistance for the reaction in wet CH_4 is $0.44 \Omega \text{ cm}^2$ on a 4.0 mg cm^{-2} GDC-impregnated LSCM anode. It showed superior polarization performance to the pure LSCM and LSCM/YSZ composite anodes.

Sin et al. [66] investigated $\text{La}_{0.6}\text{Sr}_{0.4}\text{Fe}_{0.8}\text{Co}_{0.2}\text{O}_3\text{--Ce}_{0.8}\text{Gd}_{0.2}\text{O}_{1.9}$ (LSCFO–CGO) composite material as an anode for the direct electrochemical oxidation of methane in intermediate temperature ceria electrolyte supported solid oxide fuel cells. A maximum power density of 0.17 W cm^{-2} was obtained at 800 °C. The anode did not show any structure degradation after the electrochemical testing and no carbon deposits was detected. After high temperature treatment in a dry methane stream in a packed-bed reactor, this material showed significant chemical and structural modifications. It is derived that the continuous supply of mobile oxygen anions from the electrolyte to the anode, promoted by the mixed conductivity of CGO at 800 °C, stabilizes the perovskite structure near the surface under SOFC operation and open circuit conditions.

Doped SrTiO_3 is also a kind of promising anode materials. Fagg et al. [67] studied the stability and mixed conductivity of La and Fe doped SrTiO_3 for potential SOFC anode materials. It was found that both physical properties and the level of mixed conduction obtained in La and Fe doped SrTiO_3 are widely influenced by the composition. In contrast to La free compositions, La containing compositions show high stability against reaction with YSZ and a closely matching thermal expansion coefficient ($\sim 1 \times 10^{-5} \text{ K}^{-1}$). Faradaic efficiency measurements for $\text{Sr}_{0.97}\text{Ti}_{0.6}\text{Fe}_{0.4}\text{O}_{3-\delta}$ and $\text{La}_{0.4}\text{Sr}_{0.5}\text{Ti}_{0.6}\text{Fe}_{0.4}\text{O}_{3-\delta}$ show ionic transference numbers in air between 5×10^{-3} to 4×10^{-2} , and 2×10^{-4} to 6×10^{-4} , respectively, decreasing with decreasing temperature. The substitution of La for Sr is observed to deplete the level of both ionic and total conductivity obtained in air.

Hui et al. [68] investigated yttrium-doped SrTiO_3 (SYT) as an anode material for solid oxide fuel cells in terms of electrical conductivity, phase stability, redox behavior, chemical compatibility with yttria-stabilized zirconia and $\text{La}_{0.8}\text{Sr}_{0.2}\text{Ga}_{0.8}\text{Mg}_{0.2}\text{O}_{2.8}$ (LSGM), thermal expansion coefficient, and fuel cell performance. With the optimized composition $\text{Sr}_{0.86}\text{Y}_{0.08}\text{TiO}_{3-\delta}$, the electrical conductivity was up to 82 S cm^{-1} at 800 °C, under oxygen partial pressure of 10^{-19} atm . A reversible change of conductivity was observed upon oxidation and reduction. The resistance to oxidation was enhanced by partially replacing Ti with transition metals such as cobalt. This material has high structural stability over a broad range of temperature (up to 1400 °C) and oxygen partial pressure ($1\text{--}10^{-20} \text{ atm}$). No phase change was found for mixtures of SYT with YSZ or LSGM sintered at 1400 °C for 10 h. The thermal expansion coefficient of doped- SrTiO_3 was determined to

be compatible with that of YSZ and LSGM. A maximum power density of 58 mW cm^2 at 900 °C was obtained.

Perovskite-type lanthanum chromites and titanates oxides substituted with alkaline earth ions are interesting candidate materials with tailored electrocatalytic properties. Mixed occupation of the B-site by varying Cr/Ti ratios gives the possibility of modification between donor and acceptor doping. Vashooka et al. [69] investigated the electrical properties of a series of $\text{La}_{1-x}\text{Ca}_x\text{Cr}_{0.5}\text{Ti}_{0.5}\text{O}_{3-\delta}$ ($x=0, \dots, 1.0$). They found that the compounds with $x \geq 0.6$ are p-type and with $x < 0.4$ n-type semiconductors at 900 °C and oxygen partial pressures between 1×10^{-15} and $0.21 \times 10^5 \text{ Pa}$. $\text{La}_{0.5}\text{Ca}_{0.5}\text{Cr}_{0.5}\text{Ti}_{0.5}\text{O}_{3-\delta}$ and $\text{La}_{0.6}\text{Ca}_{0.4}\text{Cr}_{0.5}\text{Ti}_{0.5}\text{O}_{3-\delta}$ change their conductivities from n-type in the range $p(\text{O}_2) < 10^{-10} \text{ Pa}$ and $p(\text{O}_2) < 10^{-5} \text{ Pa}$, respectively, to p-type in more oxidizing atmosphere. For the compound with $x=0.5$, its conductivities are changed between n- and p-type. In more reducing conditions where the ratio $\text{Ti}^{4+}/\text{Ti}^{3+}$ acts, they are n-type semiconductors, and in more oxidizing where the ratio $\text{Cr}^{3+}/\text{Cr}^{4+}$ acts, they are p-type semiconductor. For the compound with $x=0.5$ in $\text{Ar}/\text{H}_2/\text{H}_2\text{O}$ gas flow ($p(\text{H}_2\text{O})/p(\text{H}_2)=0.53$) at 900 °C, a maximum conductivity of about 1 S cm^{-1} was observed.

Pudmich et al. [70] also investigated several perovskites based on lanthanum chromite and strontium titanate used as anodes in solid oxide fuel cells. They found perovskites containing lanthanides, partially substituted by alkaline-earth elements and transition metals like Cr, Ti, Fe or Co, showed a very broad range of physical properties. High conductivity was obtained with titanium-rich materials, in the case of chromium-rich samples the conductivity dropped under reducing conditions. Impedance measurements showed an activity of the $\text{La}_{0.7}\text{Sr}_{0.3}\text{Cr}_{0.8}\text{Ti}_{0.2}\text{O}_3$ perovskite electrode towards hydrogen oxidation, but the performance of the electrode is still poor compared to that of Ni–YSZ cermet anodes.

Marina et al. [71] investigated (La,Sr) TiO_3 doped with several transition metals (Ni, Co, Cu, Cr and Fe) and Ce. They found the most effective among these dopants is cerium, which significantly decreases the polarization resistance, although iron also produces modest improvements. For (La,Sr)(Ti,Ce) O_3 , the anode polarization resistances of $0.2 \Omega \text{ cm}^2$ at 850 °C and $1.3 \Omega \text{ cm}^2$ at 700 °C were measured in wet (3% H_2O) hydrogen. It was demonstrated that doped strontium titanate-based anodes are tolerant to oxygen, carbon and sulfur containing atmospheres. In addition, Lepe et al. [72] investigated $\text{Ln}_{2/3-x}\text{TiO}_{3-3x/2}$ ($\text{Ln}=\text{La, Pr and Nd}$) as SOFC anodes. Mashkina et al. [73] investigated the electrical conductivity of Fe-doped BaTiO_3 system.

Vernoux et al. [74] investigated the performances of $\text{La}(\text{Sr})\text{Cr}(\text{Ru},\text{Mn})\text{O}_{3-\delta}$ defective perovskite materials as an anode material. By inserting ruthenium in the B site, the catalytic activity of this material for the steam reforming of methane has been improved. Catalytic performances are stable, and no carbon deposit was detected, even after 300 h of operation in a reactive mixture containing more methane than steam. It also has shown that the insertion of manganese in the B site accelerates the electrochemical oxidation of hydrogen compared with the strontium-doped lanthanum chromite. It indicated that these

perovskite materials are potential candidates as SOFC anode materials for implementing gradual internal reforming (GIR) of methane.

$\text{La}_{0.9}\text{Sr}_{0.1}\text{Ga}_{0.8}\text{Mg}_{0.2}\text{O}_{2.85}$ (LSGM) has been identified as a superior oxide-ion electrolyte [75–78], it has an oxide-ion conductivity $\sigma_o \geq 0.1 \text{ S cm}^{-1}$ at 800°C , good chemical stability, negligible electronic conduction over a broad range of oxygen partial pressures, and a stable oxide-ion conductivity over time at 600°C in preliminary aging tests. Therefore, several studies on anode materials used for LSGM electrolyte based SOFC were also carried out. Similar to YSZ based SOFCs, Huang et al. [79] have studied Ni–LSGM composite used as the anode for LSGM based SOFCs. However, the observed anodic overpotentials were high and the cell performance showed degradation with time. Studies of the anode-electrolyte interface and the reactivity of NiO and LSGM suggest better anode performances can be obtained with a buffer layer that prevents formation of LaNiO_3 . To introduce electronic conduction while maintaining the existing ionic conduction, Chen et al. [80] studied transition metal oxide doped lanthanum gallates used as MIEC electrodes. They found that $\text{La}_{0.9}\text{Sr}_{0.1}\text{Ga}_{0.8}\text{M}_{0.2}\text{O}_3$ ($\text{M}=\text{Co}, \text{Mn}, \text{Cr}, \text{Fe},$ or V) displayed not only higher conductivity but also better sinterability than that of LSGM. Among the doped LaGaO_3 studied, Co-doped LaGaO_3 exhibits the highest conductivity in air and Mn-doped LaGaO_3 exhibits the highest conductivity in H_2 , implying that the former may be used as a cathode whereas the latter may be used as an anode for LSGM-based SOFCs. Electrochemical measurements using an oxygen concentration cell indicate that $\text{La}_{0.9}\text{Sr}_{0.1}\text{Ga}_{0.8}\text{Mn}_{0.2}\text{O}_3$ is a MIEC with significant ionic conduction whereas $\text{La}_{0.9}\text{Sr}_{0.1}\text{Ga}_{0.8}\text{Co}_{0.2}\text{O}_3$ is a MIEC with overwhelming electronic conduction.

The new materials design concepts are also introduced to improve properties of the present materials. Recently, Ruiz-Morales et al. [81] used a novel design concept of inducing functionality through disorder of extended defects to enable fuel cells to more efficiently operating with CH_4 . They substitute Ti in LaSrTiO_3 with Ga and Mn to induce redox activity and allow more flexible coordination. Using $\text{La}_4\text{Sr}_8\text{Ti}_{11}\text{Mn}_{0.5}\text{Ga}_{0.5}\text{O}_{37.5}$ as an anode, the maximum powder density reached 0.35 W cm^{-2} at 950°C with wet CH_4 as a fuel.

2.2.3. Tungsten bronze anode materials

Oxides with the general formula $\text{A}_2\text{BM}_5\text{O}_{15}$ (with $\text{M}=\text{Nb}, \text{Ta}, \text{Mo}, \text{W}$, and A or $\text{B}=\text{Ba}, \text{Na}$, etc.) show a tetragonal tungsten bronze structure (TTB) or an orthorhombic tungsten bronze structure (OTB) [82]. The structure of tungsten bronze type compounds is shown in Fig. 5 [83]. These oxides can be described by a framework of MO_6 octahedra sharing summits, delimiting tunnels of pentagonal, square and triangular sections.

Slater et al. [84,85] investigated materials with the composition $(\text{Ba}/\text{Sr}/\text{Ca}/\text{La})_{0.6}\text{M}_x\text{Nb}_{1-x}\text{O}_{3-8}$ ($\text{M}=\text{Mg}, \text{Ni}, \text{Mn}, \text{Cr}, \text{Fe}, \text{In}, \text{Ti}, \text{Sn}$) used as anode materials for solid oxide fuel cells. They found that the compounds (with $\text{M}=\text{Cr}, \text{Mn}, \text{Fe}, \text{Ni}, \text{Sn}$) are not to be suitable for anode materials, either because of poor oxygen exchange kinetics, possibly due to low oxide-ion conductivity or because of partial decomposition on prolonged heat treatment at 1000°C in reduction atmospheres. However, the compounds

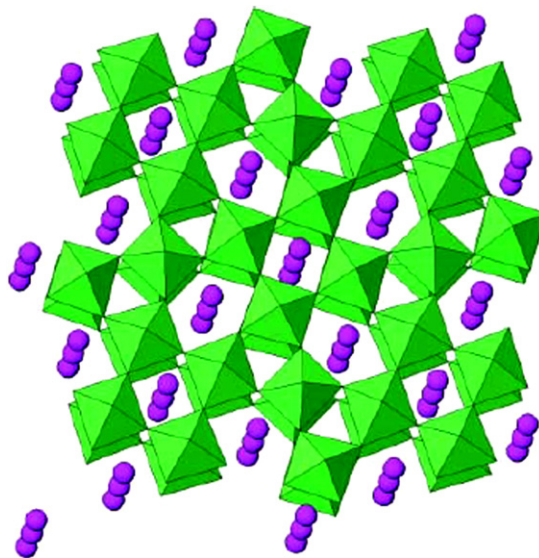


Fig. 5. The tungsten bronze structure [83].

(with $\text{M}=\text{Mg}$ or In) showed quite good conductivity characteristics and were stable under the prolonged reduction treatment, which are potential anodes for SOFCs.

Kaiser et al. [86] studied a wide range of different materials with tungsten bronze structures and the formula $(\text{Ba}/\text{Sr}/\text{Ca}/\text{La})_{0.6}\text{M}_x\text{Nb}_{1-x}\text{O}_{3-8}$ ($\text{M}=\text{Mg}, \text{Ni}, \text{Mn}, \text{Cr}, \text{Fe}, \text{In}, \text{Ti}, \text{Sn}$) used as the anode in SOFCs. They found that $\text{Sr}_{0.2}\text{Ba}_{0.4}\text{Ti}_{0.2}\text{Nb}_{0.8}\text{O}_3$ exhibits the highest electronic conductivity of about 10 S cm^{-1} at $p(\text{O}_2)=10^{-20}$ atm and at 930°C .

2.2.4. Pyrochlore anode materials

The pyrochlore-type oxides, $\text{A}_2\text{B}_2\text{O}_7$, can be derived from fluorite, by removing 1/8 of the oxygens, ordering the two cations and ordering the oxygen vacancies. The structure of pyrochlore-type oxides is shown in Fig. 6. The pyrochlore structures oxides, $\text{Gd}_2\text{Ti}_2\text{O}_7$ (GT), were also considered for use in solid oxide fuel cells [87–89]. By replacing some of

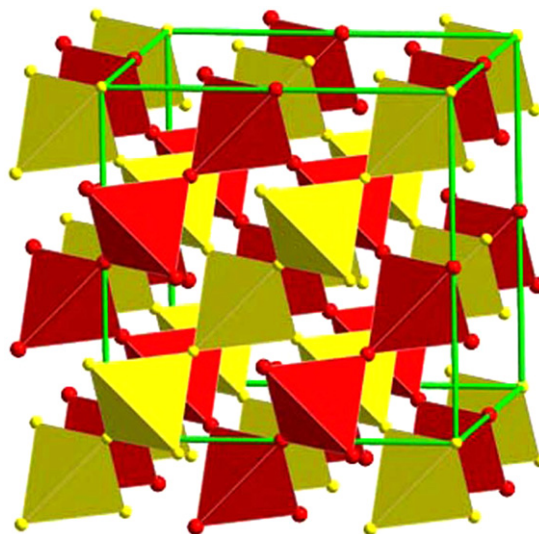


Fig. 6. The pyrochlore, $\text{A}_2\text{B}_2\text{O}_7$ structure.

the Gd^{3+} with Ca^{2+} , oxygen vacancies in the A_2O network are created, significantly increasing the ionic conductivity. At $1000^\circ C$, the ionic conductivity of $(Gd_{0.98}Ca_{0.02})_2Ti_2O_7$ is about $10^{-2} S cm^{-1}$, which is comparable to YSZ [90,91]. Mo doped GT has been shown to have a very high mixed ionic and electronic conductivity under reducing conditions, making it suitable as an anode material [92]. It was found that the electrical conductivity of $Gd_2(Ti_{1-x}Mo_x)_2O_7$ is about $70 S cm^{-1}$ and $25 S cm^{-1}$ for $x=0.7$ and 0.5 , respectively, at $p(O_2)$ around 10^{-20} atm. However, this pyrochlore solid solution is only stable at a certain $p(O_2)$ range at high temperature.

Mixed ionic electronic conductivity may be obtained for zirconates containing cations that may change valences with changing oxygen partial pressure. Mogensen et al. [93] investigated three different pyrochlore systems that are (a) $Gd_2Ti_2O_7$ modified by Mo, (b) $Pr_2Zr_2O_{7\pm\delta}$ modified by the multivalent cations Mn and Ce on the Zr-site, and (c) $Pr_2Sn_2O_{7\pm\delta}$ modified by In on the Sn-site. It is indicated that the pyrochlore solid solution $Gd_2TiMoO_{7\pm\delta}$ may be a possible candidate as an anode material in a SOFC based on a YSZ electrolyte. By optimizing the composition, these materials may be achieved an extension of the $p(O_2)$ range with stable pyrochlore structure and an increase in the total electrical conductivity.

2.3. Sulfur tolerant anode materials

Matsusaki et al. [22] studied the effect of process variables on the degree of H_2S poisoning effect for Ni based anodes by cell impedance analysis. They found that the SOFCs utilize Ni–YSZ cermet anodes are susceptible to poisoning by sulfur contents as low as 2 ppm H_2S at 1273 K. While the performance loss is reversible at H_2S concentrations less than 15 ppm, the poisoning effect became more significant at lower cell operating temperatures and that poisoning time was relatively constant at low H_2S concentrations (<100 ppm). Their work also concluded relaxation times (for H_2S poisoning) decreased with increasing operating temperature. Therefore, it is highly desirable to develop anode materials that are not deactivated by sulfur-containing fuel gases.

The desired sulfur tolerant anode materials must be electronically conductive, chemically and thermally stable, and catalytically active for the oxidation of H_2S , H_2 and CO. Wang et al. [94] prepared $Y_{0.9}Ca_{0.1}FeO_3$ (CYF) based sulfide material by exposing CYF to a gas mixture of 96% H_2 and 4% H_2S at $900^\circ C$, and they further obtained lithiated sulfide. They studied the performances of the lithiated sulfide material as the anode in H_2S -containing gases. They found the addition of lithium into the sulfides significantly increases the electrical conductivity but does not lead to a significant change in phase structure. Its conductivity was about $0.02 S cm^{-1}$ at $650^\circ C$. However, the catalytic activity and long-term stability of this material as electrodes are not studied.

He et al. [95] demonstrated the high sulfur tolerance of Cu– CeO_2 –YSZ anodes operated at lower temperature using H_2 fuel containing H_2S impurities. They found that H_2S levels up to 450 ppm had no effect on anode performance at $800^\circ C$. At higher H_2S concentrations, anode failure was observed, which

are attributed to the reaction of the CeO_2 with H_2S to form Ce_2O_2S .

Mukundan et al. [96] studied the sulfur tolerance of YSZ/ $La_{1-x}Sr_xBO_3$ (B = Mn, Cr, Ti) anode materials in a H_2/H_2O fuel containing H_2S at $1000^\circ C$. They found the $Sr_{0.6}La_{0.4}TiO_3/YSZ$ (50/50 wt.%) anode showed no degradation in the presence of up to 5000 ppm of H_2S in a hydrogen fuel. This anode was also able to operate for 8 h with 1% H_2S as a fuel and showed no degradation when the fuel was switched back to hydrogen.

Recently, Zha et al. [97] reported a pyrochlore-based anode material $Gd_2Ti_{1.4}Mo_{0.6}O_7$ showed remarkable tolerance to sulfur-containing fuels. In a fuel gas mixture of 10% H_2S and 90% H_2 , the anode/electrolyte interfacial resistance was only $0.2 \Omega cm^2$, demonstrating a peak power density of $342 mW cm^{-2}$. The fuel cell operated under these conditions for 6 days without any observable degradation, suggesting that this material have potential to make SOFCs powered by readily available sulfur-containing fuels.

Cheng et al. [98] analyzed the stability of various candidate materials for tolerance to sulfur in SOFC anode atmosphere using principles of thermodynamics. Their results help to rule out a large number of candidates such as most transition metal carbides, borides, nitrides, and silicides. Estimation of the thermochemical data for oxides with perovskite structure provides valuable predictions about the stability of those materials.

3. The development of kinetics, reaction mechanism and models of anode

Understanding the reaction mechanism and kinetics that occur on the anode is very important for the development and optimization of anode materials. The kinetics includes the kind of the chemical and of the electrochemical reactions as well as their reaction rates, the surface species, and the electrochemical parameters, such as reaction rate constants, surface coverages, and sticking coefficients. Detailed knowledge on each of these aspects allows, in principle, to determine the limitations of the fuel cell processes with regard to the electrochemistry. The main focus on the kinetics of anodes is to find the rate limiting reaction step(s) of the anodic process. This information is important, since the performance of an electrode could be considerably enhanced, if the limiting processes are identified. The electrode could then be specifically designed so that the limitations can be reduced or even avoided.

In the last decade, numerous mechanistic theories have been argued to identify the rate-controlling mechanism under various operating conditions [99], including reactivities and charge transfer [16,100–106], surface diffusion [102,104,106,107], adsorption [102,110], sintering and/or impurities [16,104,108,109], hydrogen desorption rates [104,110], catalytic effects of water [110], the role of the YSZ support [16], and others.

Mogensen and Yokokawa et al. [16,106,111] summarized the anodic oxidation of hydrogen can be limited by several processes: (i) electrochemical and chemical reaction steps at the TPB, (ii) physical transport restrictions for electrons and oxide ions in the solid structure (such as the reactions:

$O^{2-} \rightarrow O_{ad} + 2e^-$), (iii) surface adsorption and (iv) surface diffusion of species (H_{ad} , O_{ad} , OH_{ad}^-) on anode surface or diffusion of H in the anode metal to the reaction sites, and (v) by gas diffusion in the anode structure. Furthermore, (vi) concentration polarization in the gas outside the anode structure can contribute to actual measurements without having any relation to the anodes investigated. One of these steps can be rate-determining for anodic reaction. Therefore, the reaction process must be clarified to minimize anodic overpotential and improved the performances of SOFCs.

Different electrochemical models mainly agree with regard to the adsorption and to the desorption behavior of hydrogen as well as to the formation of hydroxyl. Major diversity is concerning the location where the chemical and the electrochemical reactions take place (either merely on the Ni surface or equally on the Ni and on the YSZ surface, respectively) as well as the reactions related to the interstitial oxygen in the YSZ, the adsorption and the desorption behavior of water, and the charge transfer step. In addition, the removal of oxygen from the YSZ is also assumed to proceed rather differently: the oxygen becomes either adsorbed onto the YSZ surface, or it forms a hydroxyl interstitial, or a negatively charged hydroxyl on the Ni surface, or water is immediately formed without any intermediate step [112].

Typically, Holtappels et al. [113,114] and Mogensen et al. [104] suggested the possible role of interstitial hydrogen and hydroxyl formation at the Ni/YSZ interfaces as shown in Fig. 7(a). Jiang et al. [102,115] found that hydrogen oxidation in Ni anodes is controlled by two electrode process on the surface of Ni particles and a charge transfer process on zirconia electrolyte surface. They considered the effects of surface reactions on YSZ surface as shown in Fig. 7(b). When H_2O is mixed with H_2 , the adsorption of H_2O occurred preferably on the Ni surface, which forms $OH-Ni$ as a reaction species. The following steps are considered as reaction processes:

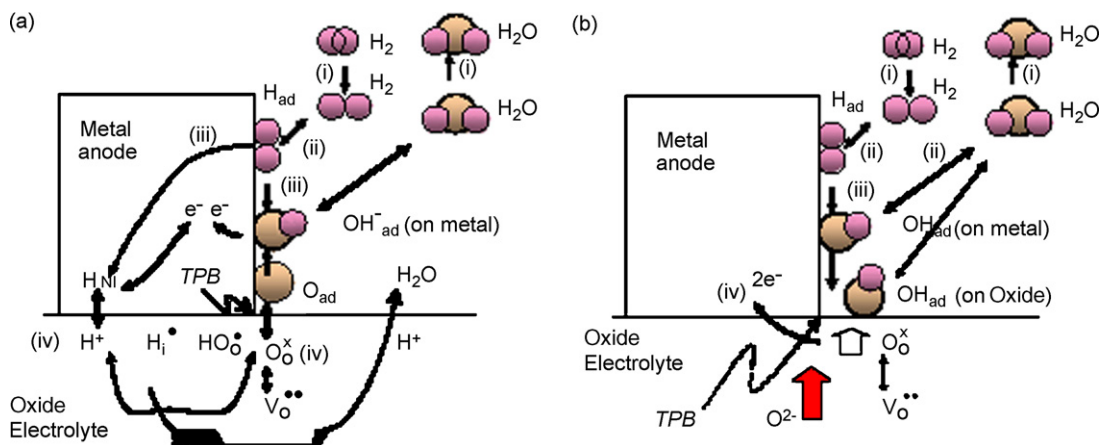
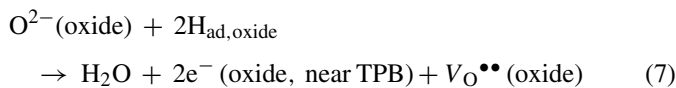


Fig. 7. Schematic diagram of possible reaction process for H_2 oxidation around the H_2 – H_2O /anode/electrolyte interfaces [111]. (a) Proposed by Holtappels et al. [113,114]; (b) proposed by Jiang and Badwal [102,115].

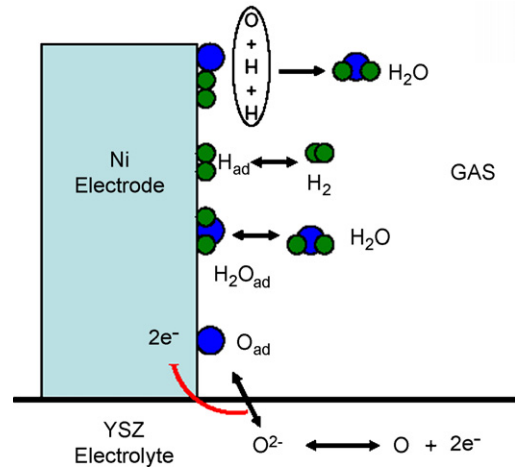


Fig. 8. Schematic diagram of the competitive adsorption mechanism on Ni/YSZ anode [116].

where S_M is an active metal surface site for adsorption, $O-S_M$ is an active metal surface site adjacent to an O_{ad} or sub-oxide. Eq. (7) is the charge transfer reaction near the TPB and the rate-determining reaction. For considering this process, the adsorption of hydrogen on the metals must be taken into account.

The schematic representations clarify the specific elemental reaction steps assumed to take place at the interface of metal anode, electrolyte, and gas phase. This indicates the important role of the three phase boundaries in the kinetics of the hydrogen oxidation reaction. Optimization of the three phase boundary areas led to the identification of the most important stages in the fabrication of anodes and in the development of the anode microstructure.

Ihara et al. [116] investigated the detailed dependence of dc polarization and interfacial conductivity of Ni/YSZ cermet anode on the partial pressure of hydrogen, $p(H_2)$. Based on the experimental results, they developed a Langmuir reaction model as shown schematically in Fig. 8, which links the chemical reactions on the anode with the electrical characteristics of the anode, such as the dc polarization and the interfacial conductivity. In their model, they assumed competitive adsorption equilibrium of

H₂, H₂O, and O on Ni surfaces at the three-phase boundary, and assumed the rate-determining step to be Langmuir-type reactions of H_{ad} with O_{ad}. They concluded that both their measured dependencies and previously published dependencies were successfully reproduced by their reaction model. Furthermore, they found the adsorption of H₂ at the TPB can be affected by the electrolyte (YSZ) at the TPB in a cermet anode.

Williford et al. [99] proposed a model to describe how concentration polarization is controlled by two localized phenomena: competitive adsorption of reactants in areas adjacent to the reactive TPB sites, followed by relatively slow surface diffusion to the reactive sites. Results suggest that future SOFC anode design improvements should focus on optimization of the reactive area, adsorption, and surface diffusion at the anode/electrolyte interface.

Recent years, some new *in situ* experimental technologies are also used to insight into the anode reaction mechanism. Traditionally, the electrochemical techniques (impedance spectroscopy and voltammetry) can provide detailed information about the rates of processes occurring *in situ*, but are not informative for assigning directly the molecular species that participate in the electrochemical reactions themselves. In contrast, optical spectroscopy is capable of identifying molecular structures present on SOFC electrode surfaces. Sum et al. [117] used Raman spectroscopy to study oxygen adsorption on Pt electrodes at temperature up to 500 °C, a process directly relevant to cathode operation in SOFCs. Lu et al. [118] examined the infrared emission from SOFC cathodes at 550 °C with a FTIR spectrometer and assigned vibrational features to surface oxide anions, based on spectral changes that depended upon applied potential. Although these studies are related to cathode reaction, they are also instructive to investigation on anode reaction mechanism in SOFCs. Recently, Pomfret [119] characterized *in-situ* chemical processes occurring in SOFC operation environments using high temperature Raman spectroscopy. The obtained information included temperature-dependent structural changes in YSZ electrolytes, reversible reduction and oxidation of Ni, carbon formation from hydrocarbon feeds, and subsequent oxidation of the deposited carbon by atmospheric H₂O.

As mentioned in the preceding sections, the main problem preventing direct oxidation hydrocarbons is that they can lead to carbon deposition at high temperatures. Recently, Kim et al. [120] studied the formation and removal of the carbonaceous deposits formed by *n*-butane and liquid hydrocarbons between 973 and 1073 K on YSZ and ceria-YSZ. They found that gas-phase, free-radical reactions can lead to the formation of high-molecular weight polyaromatic compound in the anodes, even when using anodes that do not catalyze the formation of carbon. Because steam does not participate in the gas-phase reactions, carbon deposits could form even at a H₂O:C ratio of 1.5, a value greater than the stability threshold predicted by thermodynamic calculations. These compounds deactivate the anode by essentially filling the pores. However, it is possible to oxidize these polyaromatic compounds using steam generated in the electrochemical reactions if the surface of the anodes contains catalytically active compounds, such as ceria. In addition, strategies that can be used to avoid carbon formation were also outlined.

Zhu et al. [121] developed a computational framework for modeling chemically reacting flow in anode-supported solid oxide fuel cells. Their model considers the coupled effects of channel flow, porous-media electrode transport, heterogeneous reforming and partial-oxidation chemistry, and electrochemistry in SOFCs operating with CH₄, H₂, and CO. They found that the electrochemical parameters of the model are in concert with experimentally measured button-cell performance operating on dilute hydrogen. The heterogeneous chemical reaction mechanism is validated through analysis of oxidative steam reforming of methane on Ni catalysts. The model can be applied to investigate alternative design and operating conditions, seeking to enhance understanding and interpretation of the underlying physical and chemical processes.

Hao et al. [122] recently developed a two-dimensional numerical model of a single-chamber solid oxide fuel cell (SCFC) operating on hydrocarbon fuels. The model is able to simulate the operation of SCFC with various geometries and under various operating conditions. It accounts for the coupled effects of gas channel fluid flow, heat transfer, porous media transport, catalytic reforming-shifting chemistry, electrochemistry, and mixed ionic–electronic conductivity. This model solves for the velocity, temperature, and species distributions in the gas, profiles of gaseous species and the coverage of surface species within the porous electrodes, and the current density profile in a SCFC stack for a specified electrical bias. They claimed the model is general, and can be used to simulate any electrode processes for which kinetics are known or may be estimated. A detailed elementary mechanism is also used to describe the reactions over the anode catalyst surface.

4. The development of cost-effective processing technologies for anode

For SOFCs commercialization, cost reduction is still a key issue. Various strategies have been adopted to achieve cost reduction, such as use of less expensive materials (for instance, preparation of powders through low cost processes), development of novel materials enabling operation at lower temperature, and optimization of fabrication processes.

The SOFCs are operated at lower temperatures, either by the development of ultra-thin dense, impermeable zirconia electrolyte films, or by the use of alternative solid electrolytes to YSZ, such as gadolinia-doped ceria or lanthanum gallate based structures. The lower operation temperature relaxes materials specifications throughout the system, permits the use of lower cost metallic structural and interconnect components. Another benefit is the diminished thermomechanical stress and reaction at these lower temperatures, significantly improving durability [1]. Lowering the operating temperatures of the SOFC would bring very significant cost benefits in terms of the scope of interconnect, manifold and sealing materials which can be used [123].

As for fabrication processes, tape calendaring, tape casting, slurry dip coating, and electrochemical vapor deposition (EVD) have been used extensively for the fabrication of a functional anode electrode or an anode support [124]. Compared with other

technologies, the investment cost for EVD apparatus is higher. In the case of electrolyte-supported cells, the fabrication of the electrolyte and electrode is dominated by tape casting and screen printing, respectively [125]. Both fabrication processes are well-established methods in the electroceramics industry and a scale-up is easily feasible. For the anode-supported cells, the substrates are predominantly produced by tape casting [126–131]. Usually an anode functional layer of a few micrometers in thickness is then deposited onto the substrate to enhance the electrochemical performance. A widely used deposition technique for the thin anode, electrolyte and cathode layers is screen printing. In some cases, vacuum slip casting [132], wet powder spraying [133], wet slurry printing [134] are also applied for the forming of anodes. For reducing cost, Siemens Power Generation has demonstrated a two-step process used to coat 100–150 μm thick nickel/YSZ over the electrolyte layer. In the first step, nickel powder slurry is applied over the electrolyte. In the second step, YSZ is grown around the nickel particles by the same EVD process as used for depositing the electrolyte. Deposition of the Ni–YSZ slurry over the electrolyte followed by sintering has also yielded anodes that are equivalent in performance to those fabricated by the EVD process; use of this non-EVD process will result in a substantial reduction in the cost of manufacturing SOFCs [135].

It is known that the conventional coating technologies, such as tape casting and screen printing, have to go through a high temperature sintering process. For large area cells, this step is a time-consuming process and will inevitably introduce a lot of defects. Recently, atmospheric plasma spraying (APS) is considered as a cost-effective way to produce solid oxide fuel cell components [136–138]. Different from vacuum plasma spray (VPS) process, APS is a coating process under normal pressure conditions. During this process, the ceramic thermal barrier coating is sprayed on the substrate by means of a robot-assisted plasma gun, which traverses repeatedly above the substrates at a specific speed. The main advantage of porous metallic supported thin coating cell fabricated by APS is to allow enlarging the cell area without sintering defect and improve its mechanical properties [137]. In addition, APS easily controls the component composition and microstructure through variation of spray parameters. Moreover, compared with other deposition techniques such as EVD and VPS, APS does not need sophisticated apparatus and controlled atmosphere which would increase the cost of fabrication. Furthermore, the high deposition rate of APS promises inexpensive and fast cell production with potential automation production lines. Another new adopted technology is Laser Reactive Deposition (LRDTM) process, which is a recent invention initially developed to fabricate high quality thick glass films for planar lightwave circuits [139]. LRDTM is a Laser Pyrolysis (LP) process for direct conversion of low-cost precursors, delivered to the reactor as an aerosol, into submicron or nanoscale particles with uniform and high rate deposition. During LP process, one or more components of the precursor stream obtain energy from the laser beam and nucleation events are initiated as the stream traverses the laser reaction zone. Horne et al. [140] recently investigated fabrication of SOFC components (Ni–8YSZ anodes, 8YSZ electrolyte, and Sr-doped LaMnO₃ cathode) by the LRDTM process from mixtures of the respec-

tive metal nitrates. Their results indicated that LRDTM process is suitable for fabrication of porous and dense layers with various compositions and tailored microstructures at high deposition rates. The LRDTM process converts low cost metal precursors into SOFC components directly, thus eliminating the need to undertake powder synthesis, calcinations, slurry preparation, tape formation and binder burnout steps which are required in conventional SOFC cell fabrication. By simplifying the manufacturing process, it achieves low SOFC stack manufacturing cost. Although different processes are used for the fabrication of anode and electrolyte in SOFCs, the main selection criteria for the future fabrication route are still the cost aspects, the potential for automation, reproducibility and precision of the different techniques [125].

5. Summary and outlook

In summary, the advantages and disadvantages of the most common Ni–YSZ cermet anodes have been discussed. The development of alternative anode materials is significant for direct utilization available hydrocarbon SOFCs and their commercialization. We introduced the research advances of several alternative anode materials with various crystal structures. Although alternative anodes that allow for the operation of SOFCs directly on hydrocarbons have been developed, hitherto, there are still some problems associated with all the alternative materials, mainly low catalytic activity compared with that of Ni. In addition, some materials are not sufficiently stable under operation conditions. The composition and microstructure of these anodes also need further optimization in order to improve their electrochemical characteristics.

The current studies on reaction mechanism and kinetics of the anode in SOFCs are mostly focused on that of H₂ on Ni–YSZ anodes. The reaction mechanism and kinetics of hydrocarbons on alternative anode should be intensively studied in the future. By means of in situ FTIR/Raman, impedance spectroscopy, and MS/GC measurements, characterization of fuel cell reactions may be beneficial for clarify the catalytic reaction mechanism occurred on the anode in SOFCs, thus to achieve design of new anode materials tolerant to carbon deposition and sulfur poisoning. In addition, development of rational numerical models to stimulate the electrochemical and thermodynamic processes occurred on electrodes in SOFCs operation environments also helps for optimizing the anode materials and improving the performances of SOFCs.

For SOFCs commercialization, cost reduction is still a key issue. Various processes have been used for the cost-effective fabrication of anode for the solid oxide fuel cells.

Acknowledgments

The authors acknowledge the financial support from the Deutsche Forschungsgemeinschaft (DFG STi 74-16/2) and the Sino-German Center for Research Promotion (GZ Nr. 210 (101/10)). We would also like to thank the referees for their constructive comments and suggestions on an earlier version of the manuscript.

References

- [1] S.C. Singhal, K. Kendall, *High Temperature Solid Oxide Fuel Cells: Fundamentals, Design, and Applications*, Elsevier, 2003.
- [2] A. Atkinson, S. Barnett, R.J. Gorte, J.T.S. Irvine, A.J. Mcevoy, M. Mogensen, S.C. Singhal, J. Vohs, *Nat. Mater.* 3 (2004) 17–27.
- [3] S. McIntosh, R.J. Gorte, *Chem. Rev.* 104 (2004) 4845–4865.
- [4] S.P. Jiang, S.H. Chan, *J. Mater. Sci.* 39 (2004) 4405–4439.
- [5] M. Mogensen, K. Kammer, *Annu. Rev. Mater. Res.* 33 (2003) 321–331.
- [6] J.W. Fergus, *Solid State Ionics* 177 (2006) 1529–1541.
- [7] Y. Ji, J. Liu, T.M. He, L.G. Cong, J.X. Wang, W.H. Su, *J. Alloys Compd.* 353 (2003) 257–262.
- [8] M. Juhl, S. Primdahl, C. Manon, M. Mogensen, *J. Power Sources* 61 (1996) 173–181.
- [9] Z.P. Shao, S.M. Haile, *Nature* 431 (2004) 170–173.
- [10] C.R. Xia, W. Rauch, F.L. Chen, M.L. Liu, *Solid State Ionics* 149 (2002) 11–19.
- [11] A. Lashtabeg, S.J. Skinner, *J. Mater. Chem.* 16 (2006) 3160–3170.
- [12] *Fuel Cell Handbook*, 7th ed., US Department of Energy, Morgantown, WV, 2004, <http://www.netl.doe.gov>.
- [13] R.J. Gorte, J.M. Vohs, *J. Catal.* 216 (2003) 477–486.
- [14] X. Wang, N. Nakagawa, K. Kato, *J. Electrochem. Soc.* 148 (2001) A565–A569.
- [15] T. Horita, K. Yamaji, N. Sakai, Y. Xiong, T. Kato, H. Yokokawa, T. Kawada, *J. Power Sources* 106 (2002) 224–230.
- [16] M. Brown, S. Primdahl, M. Mogensen, *J. Electrochem. Soc.* 147 (2000) 475–485.
- [17] C.W. Tanner, K.-Z. Fung, A.V. Virkar, *J. Electrochem. Soc.* 144 (1997) 21–30.
- [18] J.R. Wilson, W. Kobsiriphat, R. Mendoza, H.Y. Chen, J.M. Hiller, D.J. Miller, K. Thornton, P.W. Voorhees, S.B. Adler, S.A. Barnett, *Nat. Mater.* 5 (2006) 541–544.
- [19] N.P. Brandon, S. Skinner, B.C.H. Steele, *Annu. Rev. Mater. Res.* 33 (2003) 183–213.
- [20] N.Q. Minh, *J. Am. Ceram. Soc.* 76 (1993) 563–588.
- [21] D.W. Dees, T.D. Claar, T.E. Easler, D.C. Fee, F.C. Mrazek, *J. Electrochem. Soc.* 134 (1987) 2141–2146.
- [22] Y. Matsuzaki, I. Yasuda, *Solid State Ionics* 132 (2000) 261–269.
- [23] W.Z. Zhu, S.C. Deevi, *Mater. Sci. Eng., A* 362 (2003) 228–239.
- [24] B.C.H. Steele, *Solid State Ionics* 129 (2000) 95–110.
- [25] E.P. Murray, T. Tsai, S.A. Barnett, *Nature* 400 (1999) 649–651.
- [26] S. Park, J.M. Vohs, R.J. Gorte, *Nature* 404 (2000) 265–267.
- [27] S. McIntosh, J.M. Vohs, R.J. Gorte, *Electrochim. Acta* 47 (2002) 3815–3821.
- [28] S. Park, R. Cracium, J.M. Vohs, R.J. Gorte, *J. Electrochem. Soc.* 146 (1999) 3603–3605.
- [29] C. Lu, W.L. Worrell, R.J. Gorte, J.M. Vohs, *J. Electrochem. Soc.* 150 (2003) A354–A358.
- [30] B.C.H. Steele, P.H. Middleton, R.A. Rudkin, *Solid State Ionics* 40/41 (1990) 388–393.
- [31] S. McIntosh, J.M. Vohs, R.J. Gorte, *J. Electrochem. Soc.* 150 (2003) A470–A476.
- [32] H. Kim, C. Lu, W.L. Worrell, J.M. Vohs, R.J. Gorte, *J. Electrochem. Soc.* 149 (2002) A247–A250.
- [33] S. Lee, J.M. Vohs, R.J. Gorte, *J. Electrochem. Soc.* 151 (2004) A1319–A1323.
- [34] Z. Xie, W. Zhu, B. Zhu, C. Xia, *Electrochim. Acta* 51 (2006) 3052–3057.
- [35] C.W. Sun, J. Sun, G.L. Xiao, H.R. Zhang, X.P. Qiu, H. Li, L.Q. Chen, *J. Phys. Chem. B* 110 (2006) 13445–13452.
- [36] N.V. Skorodumova, S.I. Simak, B.I. Lundqvist, I.A. Abrikosov, B. Johansson, *Phys. Rev. Lett.* 89 (2002) 166601.
- [37] O.A. Marina, M. Mogensen, *Appl. Catal. A* 189 (1999) 117–126.
- [38] M. Suzuki, H. Sasaki, S. Otsoshi, in: F. Grosz, P. Zegers, S.C. Singhal, O. Yamamoto (Eds.), *Proceedings of the Second International Symposium of SOFC's*, Athens, 1991, p. 323.
- [39] M.J. Saeki, H. Uchida, M. Watanabe, *Catal. Lett.* 26 (1994) 149–157.
- [40] T. Hibino, A. Hashimoto, M. Yano, M. Suzuki, M. Sano, *Electrochim. Acta* 48 (2003) 2531–2537.
- [41] T. Hibino, A. Hashimoto, K. Asano, M. Yano, M. Suzuki, M. Sano, *Electrochem. Solid-State Lett.* 5 (2002) A242–A244.
- [42] Z. Zhan, S.A. Barnett, *Science* 308 (2005) 844–847.
- [43] C.W. Sun, Z. Xie, C.R. Xia, H. Li, L.Q. Chen, *Electrochem. Commun.* 8 (2006) 833–838.
- [44] E. Ramirez-Cabrera, A. Atkinson, D. Chadwick, *Solid State Ionics* 136 (2000) 825–831.
- [45] V. Antonucci, M.L. Faro, D.L. Rosa, G. Monforte, A.S. Arico, P. Antonucci, *Proceedings International Hydrogen Energy Congress and Exhibition IHEC 2005*, Istanbul, Turkey, July 13–15, 2005.
- [46] T. Hibino, A. Hashimoto, M. Yano, M. Suzuki, S. Yoshida, M. Sano, *J. Electrochem. Soc.* 149 (2002) A133–A136.
- [47] K. Ahn, H.P. He, J.M. Vohs, R.J. Gorte, *Electrochem. Solid-State Lett.* 8 (2005) A414–A417.
- [48] M. Wisniewski, A. Boreave, P. Gelin, *Catal. Commun.* 6 (2005) 596–600.
- [49] X.F. Ye, B. Huang, S.R. Wang, Z.R. Wang, L. Xiong, T.L. Wen, *J. Power Sources* 164 (2007) 203–209.
- [50] S.W. Tao, J.T.S. Irvine, *Solid State Chem.* 165 (2000) 12–18.
- [51] K. Kobayashi, Y. Kai, S. Yamaguchi, N. Fukatsu, T. Kawashima, Y. Iguchi, *Solid State Ionics* 93 (1997) 193–199.
- [52] C. Wang, W.L. Worrell, S. Park, J.M. Vohs, R.J. Gorte, *J. Electrochem. Soc.* 148 (2001) A864–A868.
- [53] D. Hirabayashi, A. Hashimoto, T. Hibino, U. Harada, M. Sano, *Electrochem. Solid-State Lett.* 7 (2004) A108–A110.
- [54] B.A. Boukamp, *Nat. Mater.* 2 (2003) 294–296.
- [55] S.W. Tao, J.T.S. Irvine, *Nat. Mater.* 2 (2003) 320–323.
- [56] S.W. Zha, P. Tsang, Z. Cheng, Z. Cheng, M.L. Liu, *J. Solid State Chem.* 178 (2005) 1844–1850.
- [57] Y.H. Huang, R.I. Dass, J.C. Denyszyn, J.B. Goodenough, *J. Electrochem. Soc.* 153 (2006) A1266–A1272.
- [58] Y.H. Huang, R.I. Dass, Z.L. Xing, J.B. Goodenough, *Science* 312 (2006) 254–257.
- [59] P. Vernoux, M. Guillo, J. Fouletier, A. Hammou, *Solid State Ionics* 135 (2000) 425–431.
- [60] J.C. Ruiz-Morales, J. Canales-Vázquez, J. Peña-Martínez, D.M. López, P. Núñez, *Electrochim. Acta* 52 (2006) 278–284.
- [61] A.L. Sauvet, J. Fouletier, *Electrochim. Acta* 47 (2001) 987–995.
- [62] A.L. Sauvet, J. Fouletier, F. Gaillard, M. Primet, *J. Catal.* 209 (2002) 25–34.
- [63] A.L. Sauvet, J.T.S. Irvine, *Solid State Ionics* 167 (2004) 1–8.
- [64] J. Liu, B.D. Madsen, Z.Q. Ji, S.A. Barnett, *Electrochem. Solid-State Lett.* 5 (2002) A122–A124.
- [65] S.P. Jiang, X.J. Chen, S.H. Chan, J.T. Kwok, *J. Electrochem. Soc.* 153 (2006) A850–A856.
- [66] A. Sin, E. Kopnin, Y. Dubitsky, A. Zaopo, A.S. Arico, L.R. Gullo, D.L. Rosa, V. Antonucci, *J. Power Sources* 145 (2005) 68–73.
- [67] D.P. Fagg, V.V. Kharton, A.V. Kovalevsky, A.P. Viskup, E.N. Naumovich, J.R. Frade, *J. Eur. Ceram. Soc.* 21 (2001) 1831–1835.
- [68] S. Hui, A. Petric, *J. Eur. Ceram. Soc.* 22 (2002) 1673–1681.
- [69] V. Vashook, L. Vasylechko, J. Zosel, U. Guth, *Solid State Ionics* 159 (2003) 279–292.
- [70] G. Pudmich, B.A. Boukamp, M. Gonzalez-Cuenca, *Solid State Ionics* 135 (2000) 433–438.
- [71] O.A. Marina, L.R. Pederson, in: J. Huijismans (Ed.), *Fifth European Solid Oxide Fuel Cell Forum, European Fuel Cell Forum, Oberrohrdorf, Switzerland, 2002*, pp. 481–489.
- [72] F.J. Lepe, J. Fernández-Urbán, L. Mestres, M.L. Martínez-Sarrión, *J. Power Sources* 151 (2005) 74–78.
- [73] E.A. Mashkina, L.A. Dunuyshkina, A.K. Demin, M. Göbbels, R. Hock, A. Magerl, in: J. Huijismans (Ed.), *Fifth European Solid Oxide Fuel Cell Forum, European Fuel Cell Forum, Oberrohrdorf, Switzerland, 2002*, pp. 695–699.
- [74] P. Vernoux, E. Djurado, M. Guillo, *J. Am. Ceram. Soc.* 84 (2001) 2289–2295.
- [75] T. Ishihara, H. Matsuda, Y. Takita, *J. Am. Chem. Soc.* 116 (1994) 3801–3803.
- [76] M. Feng, J.B. Goodenough, *Eur. J. Solid State Inorg. Chem.* 31 (1994) 663–672.

- [77] K.Q. Huang, M. Feng, J.B. Goodenough, *J. Am. Ceram. Soc.* 79 (1996) 1100–1104.
- [78] K.Q. Huang, M. Feng, J.B. Goodenough, M. Schmerling, *J. Electrochem. Soc.* 143 (1996) 3630–3636.
- [79] K. Huang, M. Feng, J.B. Goodenough, C. Milliken, *J. Electrochem. Soc.* 144 (1997) 3620–3624.
- [80] Fanglin Chen, Liu. Meilin, *J. Solid State Electrochem.* 13 (1998) 7–14.
- [81] J.C. Ruiz-Morales, J. Canales-vazquez, C. Savaniu, D. Marrero-Lopez, *Nature* 439 (2006) 568–571.
- [82] M. Tournoux, M. Ganne, Y. Piffard, *J. Solid State Chem.* 96 (1992) 141–153.
- [83] S.W. Tao, J.T.S. Irvine, *Chem. Rec.* 4 (2004) 83–95.
- [84] P.R. Slater, J.T.S. Irvine, *Solid State Ionics* 124 (1–2) (1999) 61–72.
- [85] P.R. Slater, J.T.S. Irvine, *Solid State Ionics* 120 (1–4) (1999) 125–134.
- [86] A. Kaiser, J.L. Bradley, P.R. Slater, J.T.S. Irvine, *Solid State Ionics* 135 (2000) 519–524.
- [87] H.L. Tuller, *J. Phys. Chem. Solids* 55 (1994) 1393–1404.
- [88] B.J. Wuensch, K.W. Eberman, C. Heremans, E.M. Ku, P. Onnerud, E.M.E. Yeo, S.M. Haile, J.K. Stalick, J.D. Jorgensen, *Solid State Ionics* 129 (2000) 111–133.
- [89] M. Pirzada, R.W. Grimes, L. Minervini, J.F. Maguire, K.E. Sickafus, *Solid State Ionics* 140 (2001) 201–208.
- [90] S. Kramer, M. Spears, H.L. Tuller, *Solid State Ionics* 72 (1994) 59–66.
- [91] S.A. Kramer, H.L. Tuller, *Solid State Ionics* 82 (1995) 15–23.
- [92] O. Porat, C. Heremans, H.L. Tuller, *Solid State Ionics* 94 (1997) 75–83.
- [93] P. Holtappels, F.W. Poulsen, M. Mogensen, *Solid State Ionics* 135 (2000) 675–679.
- [94] S.Z. Wang, M.L. Liu, J. Winnick, *J. Solid State Electrochem.* 5 (2001) 188–195.
- [95] H.P. He, R.J. Gorte, J.M. Vohs, *Electrochem. Solid-State Lett.* 8 (2005) A279–A280.
- [96] R. Mukundan, E.L. Brosha, F.H. Garzon, *Electrochem. Solid-State Lett.* 7 (2004) A5–A7.
- [97] S.W. Zha, Z. Cheng, M.L. Liu, *Electrochem. Solid-State Lett.* 8 (2005) A406–A408.
- [98] Z. Cheng, S.W. Zha, M.L. Liu, *J. Electrochem. Soc.* 153 (2006) A1302–A1309.
- [99] R.E. Williford, L.A. Chick, G.D. Maupin, S.P. Simner, J.W. Stevenson, *J. Electrochem. Soc.* 150 (2003) A1067–A1072.
- [100] J. Mizusaki, H. Takagawa, K. Isobe, M. Tajika, I. Koshiro, H. Maruyama, K. Hirano, *J. Electrochem. Soc.* 141 (1994) 1674–1683.
- [101] D. Kek, N. Bonanos, M. Mogensen, S. Pejovnik, *Solid State Ionics* 131 (2000) 249–259.
- [102] S.P. Jiang, S.P.S. Badwal, *Solid State Ionics* 123 (1999) 209–224.
- [103] B. de Boer, M. Gonzales, H.J.M. Bouwmeester, H. Verweij, *Solid State Ionics* 127 (2000) 269–276.
- [104] M. Mogensen, S. Skaarup, *Solid State Ionics* 86–88 (1996) 1151–1160.
- [105] P. Holtappels, L.G.J. de Haart, U. Stimming, *J. Electrochem. Soc.* 146 (1999) 1620–1625.
- [106] P. Holtappels, I.C. Vinke, L.G.J. de Haart, U. Stimming, *J. Electrochem. Soc.* 146 (1999) 2976–2982.
- [107] J. Mizusaki, H. Takagawa, T. Saito, K. Kamitani, T. Yamamura, K. Hirano, S. Ehara, T. Takagi, T. Hikita, M. Ippommatsu, S. Hakagawa, K. Hashimoto, *J. Electrochem. Soc.* 141 (1994) 2129–2134.
- [108] K.V. Jensen, S. Primdahl, I. Chorkendorff, M. Mogensen, *Solid State Ionics* 144 (2001) 197–209.
- [109] H. Itoh, T. Yamamoto, M. Mori, T. Horita, N. Sakai, H. Yokokawa, M. Dokiya, *J. Electrochem. Soc.* 144 (1997) 641–646.
- [110] B. Bieberle, L.P. Meier, L.J. Gauckler, *J. Electrochem. Soc.* 148 (2001) A646–A656.
- [111] T. Horita, H. Kishimoto, K. Yamaji, Y.P. Xiong, N. Sakai, M.E. Brito, H. Yokokawa, *Solid State Ionics* 177 (2006) 1941–1948.
- [112] A. Bieberle, Ph.D. Thesis, Swiss Federal Institute of Technology, Zürich, 2000.
- [113] P. Holtappels, L.G.J. De Haart, U. Stimming, *J. Electrochem. Soc.* 146 (1999) 1620–1625.
- [114] P. Holtappels, I.C. Vinke, L.G.J. De Haart, U. Stimming, *J. Electrochem. Soc.* 146 (1999) 2976–2982.
- [115] S.P. Jiang, S.P.S. Badwal, *J. Electrochem. Soc.* 144 (1997) 3777–3784.
- [116] M. Ihara, T. Kusano, C. Yokoyama, *J. Electrochem. Soc.* 148 (2001) A209–A219.
- [117] O.S.N. Sum, E. Djurado, T. Pagnier, N. Rosman, C. Roux, E. Siebert, *Solid State Ionics* 176 (2005) 2599–2607.
- [118] X. Lu, P.W. Faguy, M.L. Liu, *J. Electrochem. Soc.* 149 (2002) A1293–A1298.
- [119] M.B. Pomfret, J.C. Owrutsky, R.A. Walker, *J. Phys. Chem. B* 110 (2006) 17305–17308.
- [120] T. Kim, G. Liu, M. Boaro, S.I. Lee, J.M. Vohs, R.J. Gorte, O.H. Al-Madhi, B.O. Dabbousi, *J. Power Sources* 155 (2005) 231–238.
- [121] H.Y. Zhu, R.J. Kee, V.M. Janardhanan, O. Deutschmann, D.G. Goodwin, *J. Electrochem. Soc.* 152 (2005) A2427–A2440.
- [122] Y. Hao, D.G. Goodwin, *J. Electrochem. Soc.* 154 (2007) B207–B217.
- [123] R.M. Ormerod, *Chem. Soc. Rev.* 32 (2003) 17–28.
- [124] P. Singh, N.Q. Minh, *Int. J. Appl. Ceram. Technol.* 1 (2004) 5–15.
- [125] F. Tietz, H.P. Buchkremer, D. Stover, *Solid State Ionics* 152/153 (2002) 373–381.
- [126] K. Honegger, E. Batawi, C. Sprecher, R. Diethelm, in: U. Stimming, S.C. Singhal, H. Tagawa, W. Lehnert (Eds.), *Proceedings of the Fifth International Symposium on Solid Oxide Fuel Cells (SOFC-V)*, The Electrochemical Society, Pennington, NJ, 1997, p. 321.
- [127] G.M. Christie, J.P.P. Huijsmans, in: U. Stimming, S.C. Singhal, H. Tagawa, W. Lehnert (Eds.), *Proceedings of the Fifth International Symposium on Solid Oxide Fuel Cells (SOFC-V)*, The Electrochemical Society, Pennington, NJ, 1997, p. 718.
- [128] D. Simwonis, H. Thulen, F.J. Dias, A. Naoumidis, D. Stöver, *J. Mater. Process. Technol.* 92–93 (1999) 107–111.
- [129] S. Primdahl, M.J. Jørgensen, C. Bagger, B. Kindl, in: S.C. Singhal, M. Dokiya (Eds.), *Proceedings of the Sixth International Symposium on Solid Oxide Fuel Cells (SOFC-VI)*, The Electrochemical Society, Pennington, NJ, 1999, p. 793.
- [130] D. Gosh, G. Wang, R. Brule, E. Tang, P. Huang, in: S.C. Singhal, M. Dokiya (Eds.), *Proceedings of the Sixth International Symposium on Solid Oxide Fuel Cells (SOFC-VI)*, The Electrochemical Society, Pennington, NJ, 1999, p. 822.
- [131] K. Föger, B. Godfrey, in: A.J. McEvoy (Ed.), *Proceedings of the Fourth European SOFC Forum*, The European Fuel Cell Forum, Oberrohrdorf, Switzerland, 2000, p. 261.
- [132] D. Stöver, U. Diekmann, U. Flesch, H. Kabs, W.J. Quadackers, F. Tietz, I.C. Vinke, in: S.C. Singhal, M. Dokiya (Eds.), *Proceedings of the Sixth International Symposium on Solid Oxide Fuel Cells (SOFC-VI)*, The Electrochemical Society, Pennington, NJ, 1999, p. 813.
- [133] N.M. Sammes, M.S. Brown, R. Ratnaraj, *J. Mater. Sci. Lett.* 13 (1994) 1124–1126.
- [134] F.J. Gardner, M.J. Day, N.P. Brandon, M.N. Pashley, M. Cassidy, *J. Power Sources* 86 (2000) 122–129.
- [135] S.C. Singhal, *Solid State Ionics* 135 (2000) 305–313.
- [136] D. Hathiramani, R. Vassen, D. Stover, R.J. Damani, *J. Therm. Spray Technol.* 15 (2006) 593–597.
- [137] S. Takenoiri, N. Kadokawa, K. Koseki, *J. Therm. Spray Technol.* 9 (2000) 360–363.
- [138] R. Zheng, X.M. Zhou, S.R. Wang, T.L. Wen, C.X. Ding, *J. Power Sources* 140 (2005) 217–225.
- [139] X.X. Bi, R.J. Mosso, S. Chiruvolu, E. Euvrard, M. Bryan, T.S. Jenks, in: S. Jian, Y. Liu (Eds.), *Proceedings of the SPIE*, Bellingham, WA, 2001, p. 71.
- [140] C.R. Horne, E. Ooi, R.B. Lynch, J.R. Mentz, W.E. McGovern, R.J. Mosso, in: S.C. Singhal, J. Mizusaki (Eds.), *Solid Oxide Fuel Cells IX*, The Electrochemical Society, Quebec City, Canada, 2005, pp. 466–475.